On Computationally Efficient Radiative Transfer Calculations for Three-dimensional Entry Problems

Amal Sahai *
AMA, Inc. at NASA Ames Research Center, Moffett Field, California 94035

Christopher O. Johnston †
NASA Langley Research Center, Hampton, Virginia 23681

The current work presents an efficient simulation framework for rigorously modeling radiative fields emanating from non-equilibrium planetary entry flows in complex three-dimensional domains. Key to this endeavor is adoption of finite-volume discretization in lieu of brute-force ray tracing. This change in conjunction with mesh sweeping and Lebedev-type quadrature for angular integration allows spatial-angular resolution of radiative transfer to be performed in a computationally tractable manner. Additionally, a new methodology has been established to build standalone reduced-order spectral databases for non-equilibrium radiative properties that can be applied to a broad range of hypersonic planetary entry problems with minimal loss in accuracy. The efficacy of the new framework has been demonstrated on the atomic nitrogen radiative system. The resulting reduced-order model requires three orders-of-magnitude fewer spectral evaluations and results in a 95% decrease in memory footprint. A comparative study for representative forebody and afterbody lines-of-sight from Stardust, FIRE II, and meteor entries into the Earth atmosphere indicates that both total intensity variation and detailed spectra can be retrieved with as few as 625 reduced-order groups (contrasting with the 100,000 frequencies in the original full set model). Similarly, three-dimensional predictions of radiative heating experienced by the Orion forebody are in excellent agreement with legacy radiation solvers while requiring only a sliver (roughly 0.5%) of computing wall time.

I. Introduction

NASA is currently planning missions with entry, descent, and landing (EDL) phases or aerocapture maneuvers involving increasingly higher velocities, e.g., Mars Sample Return - Earth Entry Vehicle (MSR-EEV) [1] and denser atmospheric conditions, e.g., Dragonfly [2]. These extreme conditions make it imperative that the various physical phenomena shaping hypersonic flight – thermochemically reactive flows, radiation, ablation – be modeled in a coupled manner in order to obtain reliable predictions for vehicle design requirements [3]. However, with regards to flow-radiation coupling, there are computational impediments to running NASA's production aerothermal analysis tools [4] and delivering simulations in design-relevant timespans for practical three-dimensional (3D) spacecraft geometries. This necessitates the introduction of simplifying assumptions in the underlying physical principles and/or descoping the analysis to a handful of points-of-interest. The lack of a comprehensive overview of radiative heating and the interaction between radiation and flowfield dynamics, in turn, contributes to larger safety factors in spacecraft designs. Thus, limited physical realism available to designers can adversely impact mission viability and payload potential.

The generalized radiative field has a complex domain of dependence with six independent variables: three spatial dimensions, two solid angle dimensions, and frequency. Additionally, photochemical behavior, encapsulated in the absorption and emission coefficients, is determined by the state of the inhomogenous, hot gaseous flow blanketing the spacecraft. NASA's current radiation tools, NEQAIR [5] and HARA [6], deal with the geometric aspect by tracking radiative transfer along bundles of lines-of-sight (LOSs) originating at specific locations of interest [7]. This approach is computationally expensive for surface heat flux calculations and becomes practically intractable for coupled simulations which require irradiance for all cells of the volume mesh used to solve flow equations (and not merely surface points). Moreover, the rapid change in radiative coefficients with frequency is resolved using a line-by-line (LBL) approach [8] or narrow-band models [9]. The use of such fine spectral discretization, usually comprising of $O(10^5 - 10^6)$ distinct frequency points, allows both the heat transfer component and induced thermochemical changes to be captured with

*Research Scientist, Aerothermodynamics Branch. Member AIAA. Corresponding author: amal.sahai@nasa.gov.
†Aerospace Engineer, Aerothermodynamics Branch. Associate Fellow AIAA.

exceptional accuracy. However, the cumulative cost of spatial-angular transfer evaluations, repeated for each frequency point, renders analysis of large-scale problems unfeasible.

The objective of the present work is to establish an alternate radiation simulation framework that could ameliorate computational constraints plaguing current NASA tools for aerothermal analysis. This would serve as the first step in making high-fidelity 3D flow-radiation coupled calculations readily available for spacecraft design studies, directly translating into improvements in spacecraft safety and mission performance. Additionally, the focus is also on interfacing with existing production software such as the radiation solvers HARA/NEQAIR and the computational fluid dynamics (CFD) code US3D [10]. In order to realize these objectives, a notable departure from legacy techniques is enacted. Finite volume-based spatial discretization coupled with mesh reordering and angular integration based on Lebedev-type quadrature is adopted which enables spatial-angular variation in radiative intensity to be rapidly computed. Furthermore, a novel methodology is devised for constructing generalized spectral reduced-order models (ROMs) that can accurately predict non-equilibrium radiation for a wide range of planetary entry problems. This paper is organized as follows: a) Sec. II details the numerical strategies for handling the spatial, angular, and spectral facets of radiation. b) Sec. III begins with applying the new spectral model-reduction methodology to the atomic nitrogen radiative system. Then, a comparative analysis on LOSs extracted from different Earth entry flowfields is presented. Finally, the new simulation framework is assessed by computing radiative heating experienced by the 3D Orion forebody. c) Sec. IV summarizes key conclusions and possible directions for future work.

II. Key Components of Efficient Radiation Computation

The fundamental governing equation, referred to as the radiative transfer equation (RTE) [11], describes the evolution of intensity (radiant energy flux per unit area per unit per unit frequency) in a given direction corresponding to a specific frequency:

$$\mathbf{\Omega} \cdot \boldsymbol{\nabla} I_\nu \quad = \quad J_\nu - \kappa_\nu I_\nu \tag{1}$$

where I_ν is the monochromatic light intensity for frequency ν along the $\mathbf{\Omega}$ direction. The opacity and emissivity for the current frequency ν are denoted by are κ_ν and J_ν, respectively. The net heat flux at a given location in space can then be obtained by integrating monochromatic intensity over the entire solid angle and frequency space $\left[\nu_i, \nu_f\right]$:

$$\mathbf{q}_{\text{rad}} = \int_{\nu_i}^{\nu_f} \oint_{4\pi} I_\nu \, \mathbf{\Omega} \, d\mathbf{\Omega} \, d\nu \tag{2}$$

The complete description of a 3D radiative field requires solving the geometric aspects of radiative transfer (*angular*, *spatial*) while accounting for frequency (*spectral*) variation in the radiative properties of the surrounding hot gas. Thus, a robust mitigation of computational costs requires addressing modeling bottlenecks associated with all three domains of dependence for radiative heat transfer.

A. Angular

The current work employs the discrete-ordinates method which solves the RTE equations for a set of discrete directions $\mathbf{\Omega}^m$ [12]. The underlying motivation is to approximate the otherwise complex angular integration by a weighted vector sum of radiative intensities along $\mathbf{\Omega}^m$ and yield the spatially varying net radiative flux (and its divergence):

$$\mathbf{q}_{\text{rad}} = \int_{\nu_i}^{\nu_f} \oint_{4\pi} I_\nu \, \mathbf{\Omega} \, d\mathbf{\Omega} \approx \int_{\nu_i}^{\nu_f} \sum_m w^m \, I_\nu^m \, \mathbf{\Omega}^m \, d\nu \tag{3}$$

where the quadrature weight and radiative intensity linked with direction $\mathbf{\Omega}^m$ are w^m and I_λ^m, respectively. Lebedev-type quadrature [13] rules are used which significantly lower the number of discrete directions required for a given polynomial order of accuracy while minimizing distortions based on ray effects and false scattering.

B. Spatial

A key differentiator underpinning the current work is a switch to efficient finite volume-based spatial discretization from the more onerous ray tracing approaches [5, 7]. This change also simplifies interfacing with existing finite-volume based CFD solvers and allows radiation/flow-field calculations to be performed in a loosely coupled manner. Finite-volume based approaches, which can draw upon mature numerical/computational strategies prevalent in CFD, have

been successfully applied for resolving radiation in a wide variety of fields such as combustion [14], medicine [15], and stellar dynamics [16]. However, their usage for studying the impact of radiative heating for hypersonic blunt body flows [17] has so far been limited. The spatial discretization and solution strategy being utilized here were first outlined in [18, 19]. A brief summary of the same is provided in the interest of completeness. Finite-volume discretization begins with first integrating Eq. (1) corresponding to direction $\mathbf{\Omega}^m$ and frequency ν over the i^{th} computational cell:

$$\int_{\mathbf{S^i}} I_\nu^m \, \mathbf{\Omega}^m \cdot d\mathbf{S} \quad = \quad \int_{V^i} \left(J_\nu - \kappa_\nu I_\nu^m \right) \, dV \, , \qquad I_\nu(\mathbf{x}, \mathbf{\Omega}^m) \; : \; I_\nu^m(\mathbf{x}) \tag{4}$$

Standard simplifications pertaining to approximating the volume (product between the value at cell center $\mathbf{x}_c^i$ and the cell volume ΔV^i) and surface integrals (summation over faces of the product between the face-centered values at $\mathbf{x}_k^i$ and the corresponding areas $\Delta \mathbf{S}_k^i$) are then introduced:

$$\sum_k I_\nu(\mathbf{x}_k^i, \, \mathbf{\Omega}^m) \, \mathbf{\Omega}^m \cdot \Delta \mathbf{S}_k^i \quad = \quad \left\{ J_\nu(\mathbf{x}_c^i) - \kappa_\nu(\mathbf{x}_c^i) \, I_\nu(\mathbf{x}_c^i, \, \mathbf{\Omega}^m) \right\} \Delta V^i \tag{5}$$

Furthermore, surface fluxes are categorized into incoming ($\mathbf{\Omega}^m \cdot \Delta \mathbf{S}_k^i < 0$) and outgoing ($\mathbf{\Omega}^m \cdot \Delta \mathbf{S}_k^i > 0$) components. First-order upwinding (also referred to as the step scheme in radiation literature [12]) is used and radiative intensities at face-centers for the outward fluxes are set equal to the cell-center values of the current cell. These steps can be condensed into the following expression for $I_\nu(\mathbf{x}_c^i, \mathbf{\Omega}^m)$:

$$I_\nu(\mathbf{x}_c^i, \, \mathbf{\Omega}^m) \quad = \quad \frac{\sum_{\forall k \ni \mathbf{\Omega}^m \cdot \Delta \mathbf{S}_k^i < 0} I_\nu(\mathbf{x}_k^i, \, \mathbf{\Omega}^m) \, |\mathbf{\Omega}^m \cdot \Delta \mathbf{S}_k^i| \, + \, J_\nu(\mathbf{x}_c^i) \, \Delta V^i}{\sum_{\forall k \ni \mathbf{\Omega}^m \cdot \Delta \mathbf{S}_k^i > 0} |\mathbf{\Omega}^m \cdot \Delta \mathbf{S}_k^i| \, + \, \kappa_\nu(\mathbf{x}_c^i) \, \Delta V^i} \tag{6}$$

Equation 6 when written for the entire computational grid forms a sparse system of linear equations. The original system can be solved more efficiently by performing "mesh sweeps" [20] which effectively transforms it into a lower triangular system and amenable to forward substitution. This procedure involves identifying the sequence (referred to as the "advance-order list") in which cells need to be accessed for a given direction while ensuring that I_ν^m for all upstream neighboring cells have already been updated. Consequently, I_ν^m for a given cell can be computed using the explicit expression provided in Eq. (6). This is also roughly analogous to marching along a discretized line-of-sight (or a characteristic), starting from a boundary surface. A potential complication with applying mesh reordering algorithms to unstructured meshes is encountering regions of computational cells with circular dependencies (often due to unavoidable mesh defects). The current framework incorporates a two-step strategy (previously tested on a plethora of complex meshes [19]) to address these anomalies. Firstly, explicit checks have been added to break out of circular ties when advance-order lists are being built. Secondly, sub-iterations, comparable to the Gauss-Seidel method, are used to accurately calculate I_ν^m for meshes with such deficiencies [14].

C. Spectral

The current study builds upon previous work [21, 22] on improving the applicability of Planck-averaging based reduced-order spectral models for non-equilibrium gas mixtures. The fundamental idea behind this model-reduction paradigm is straightforward; larger groups of individual frequencies are defined from a detailed spectral model (referred to as the "Full Set" model in the present work). The governing equations for the group-wise intensity $\hat{I}_i$ can then simply be obtained by integrating the monochromatic RTE (Eq. (1)) over the set of frequencies $\{\nu_i\}$ encompassing the given reduced-order group:

$$\begin{aligned} \int\limits_{\nu \in \{\nu_i\}} \left(\mathbf{\Omega} \cdot \boldsymbol{\nabla} I_\nu \, + \, \kappa_\nu I_\nu \, - \, J_\nu \right) d\nu \quad &= 0 \\ \Rightarrow \qquad \mathbf{\Omega} \cdot \boldsymbol{\nabla} \hat{I}_i \, + \, \hat{\kappa}_i \hat{I}_i \, - \, \hat{J}_i \quad &= 0 \end{aligned} \tag{7}$$

The exact value of the group-wise emissivity is simply $\hat{J}_i = \int J_\nu \, d\nu$. On the other hand, the closure for group-wise absorption coefficient, $\hat{\kappa}_i = \int \kappa_\nu \, I_\nu \, d\nu \, / \int I_\nu \, d\nu$, requires a knowledge of the spectral intensity I_ν distribution and its assumed form varies with choice of reduced-order models. Planck-averaging prescribes I_ν equal to Planck blackbody intensity, evaluated at the appropriate local flowfield temperature, while computing group-averaged opacity. Furthermore, Planck-averaging based reduced-order models have been applied to a wide range of complex, non-equilibrium, and

optically intermediate to thick radiative problems [21, 23]. The high degree of veracity when compared to detailed narrow-band or line-by-line (LBL) predictions can be attributed to Planck-averaging being a constrained maximum entropy closure method [24], *i.e*., a piece-wise maximum entropy reconstruction of spectral intensity with only the summation of moments (total group intensity) being available [22, 25].

The comparative analysis presented in [22] indicates that Planck-averaging in conjunction with the standard multi-band opacity binning approach (MBOB) — reduced-order groups defined as non-overlapping frequency intervals (referred to as bands) and then sub-divided into bins based on intervals in the absorption coefficient space – is fundamentally equivalent to popular statistics-driven approaches such as k-distribution [11] or theory of homogenization [26]. As demonstrated in [22], a far more effective strategy for addressing the shortcomings of existing reduced-order spectral models is to engineer novel grouping strategies, *i.e*., the criteria for dividing spectral points into groups, that are more reflective of the dynamics of non-equilibrium radiation. This is pursued in [22] by comparing the exact full set solutions with the corresponding expressions for reduced-order systems. The resulting physically consistent grouping procedure retains the MBOB paradigm but now defines bands as equal logarithmic intervals in the J_ν space which are further sub-divided into bins consisting of equal logarithimic intervals in the $(J_\nu\ \kappa_\nu)$ space.

Although the new model-reduction methodology delineated in [22] consistently provides a two to four orders-of-magnitude decrease in required spectral evaluations with respect to narrow-band and LBLS methods, it still suffers from a few noticeable shortcomings. The construction of Planck-averaged models in the examples presented previously relied on having access to the full set of J_ν and κ_ν data for all points in the LOS. Additionally, each instance of a reduced-order model was calibrated to a single LOS with no consideration for how accurately it would capture the dynamics of another LOS or an altogether different flow problem. These issues need redressing in order to ensure reduced-order spectral models can be exploited for practical problems with minimal user or case-specific inputs. The present work enshrines certain tenets in order to realize truly general-purpose ROM databases: 1) construction of reduced-order spectral model needs to be completed before flow simulations and radiative transfer calculations are performed (*a priori*), 2) flowfield-specific data will not be made available for model-reduction (*generalizability*), and 3) the resulting database should be easy to store and evaluate (*portability*).

Since the grouping scheme — mapping between full set frequencies and reduced-order groups — remains invariant in space, it operates on reference values for the absorption κ_ν^{ref} and emission J_ν^{ref} coefficients at a given frequency ν. Previous research including that by the current authors [22, 27] typically defines the reference state by averaging the distribution of κ_ν^{ref}, J_ν^{ref} throughout the flowfield. This approach is now considered unacceptable because it would violate the *a priori* and *generalizability* requirements listed before. Instead, numerical investigations on the matter have yielded a valuable insight. The grouping procedure only requires a rough "snapshot" of the entire original system that is sufficiently representative of the relative differences in κ_ν^{ref}, J_ν^{ref} values between individual frequencies. Thus, in lieu of estimating frequency-wise variation by considering actual flowfields the same information can be gleaned by an unweighted logarithmic average of radiative properties obtained for a limited set of gaseous states – temperature, partial density, total pressure – that roughly span the possible range of flow conditions to be encountered during simulations. The current framework incorporates the use of look-up tables both for the input full set databases and the outputted ROM models. The same discrete flow conditions for which radiative properties are tabulated can be conveniently re-used during averaging to establish the reference state.

In similar vein, a new two-step grouping procedure has been effected to ensure the same ROM can be applied to the widest variety of test cases. First, the procedure from [22] involving bands based on J_ν and bins based on $(J_\nu\ \kappa_\nu)$ is repeated. A deeper analysis of the composition of reduced-order groups revealed that since band/bin definitions are based on equal logarithmic intervals, a significant number of them can remain empty. Consequently, a follow-up routine has been added. Reduced-order groups with the largest spread, quantified using standard deviation, in $\nu \times \log(\nu)$ values are identified and bisected till all empty groups are filled up. The aforementioned heuristic forces frequencies with similar values of black body radiation together, thereby enabling better representation of group absorptivity using Planck-averaging. Additionally, numerical testing points to this approach retaining more accuracy when compared to other standard strategies for ensuring non-empty groups such as assigning an equal number of frequencies to each group.

The *portability* prerequisite is fulfilled by a careful organization of ROM data in the form of a look-up table. The present structure closely follows that put forth by preceding work on rendering Planck-averaging compatible with non-Boltzmann internal population distributions [21]. The ROM look-up table is organized in the the following hierarchy:

I) Type of radiative process (*e.g*., bound-bound, bound-free, free-free)

    II) List of transitions between specific internal levels

III) Discrete physical conditions (*e.g.*, temperatures, electron number density, pressure) which also capture effects such as line-broadening

IV) Level number density normalized coefficients for absorption, spontaneous emission, and induced emission for each group.

Tabulating normalized radiative coefficients originating in different radiative transitions separately allows easy recovery of radiative properties after scaling by the appropriate level number densities. This usually involves multiplying the absorption coefficient by the number density of the lower level for the transition and the emission coefficients by those of the upper level or the free electrons and ionized state. The population densities of internal energy levels are no longer an input dimension for the look-up table which markedly reduces storage footprint and evaluation cost. Furthermore, the same ROM database can be employed for both Boltzmann and non-Boltzmann population distributions without running into the curse of dimensionality. It should be noted that linear interpolation is used to obtain the normalized coefficients for arbitrary flow conditions. The use of higher-order interpolation schemes did not result in any appreciable increase in accuracy and have been ignored to aid stability. The standard workflow for determining group-wise $\hat{\kappa}_i$ and $\hat{J}_i$ now consists of looping over different radiative processes, summing contributions from individual transitions after appropriately interpolating and scaling normalized coefficients.

III. Results

The principal deliverable of the present work is a radiation solver, titled Non-Equilibrium RadiatiOn (NERO), incorporating finite volume spatial discretization, mesh reordering, Lebedev-type quadrature, and reduced-order spectral models that can link with existing NASA aerothermal analysis software. Although NERO's genesis predates this effort [19], the current version has been rewritten from the ground up. It possesses a suite of new features for handling large meshes and complex flow systems, key amongst them being different parallelization schemes depending on memory availability, novel boundary conditions for exploiting planar/axis symmetry, and an object-oriented-based toolset for rapidly adding new radiative or chemical systems. Another important highlight are the flow-agnostic, *a priori* constructed, portable ROM databases that can just as easily be plugged into other RTE solvers. The new radiation solver NERO runs in conjunction with US3D [10], one of NASA's workhorse CFD tools, to compute radiative heat flux and radiation-induced energy/mass source terms for the flowfield (in the case of 2-way coupled simulations). The US3D finite-volume flow code solves the chemically reacting non-equilibrium Navier-Stokes equations on unstructured grids using the implicit data-parallel line-relaxation method and a wide range of numerical flux functions.

The new spectral model-reduction methodology has been applied to radiation from atomic nitrogen [28]. The spectral range, covering the infrared (IR), visible (V), ultraviolet (UV), and vacuum ultraviolet (VUV) regions, has been discretized using approximately 100,000 frequencies in the full set and accounts for bound-bound, bound-free, and free-free transitions. The large spectral span, diverse radiative characteristics, and ensuing complexities due to non-Boltzmann electronic populations for N provide a challenging test for wide-band models with exceptionally limited degrees of freedom being envisaged in the current work. The number of groups in the reduced-order models created for atomic nitrogen have been varied between $400 - 625$, representing a two to three orders-of-magnitude lowering of spectral evaluations. Storage requirements, also illustrative of RAM usage during simulations, have seen a similar drop from roughly 2.5 Gb for the full-set to 125 Mb for the ROM databases. The section begins with benchmarking the accuracy of the reduced-order models along LOSs extracted from a variety of flow problems. This is followed by an investigation into 3D radiative heating experienced by the Orion forebody.

A. Line-of-Sight Analysis

Three hypersonic Earth-entry scenarios and the accompanying radiative field due to atomic nitrogen are presented here: 1) Stardust probe, 2) FIRE II experiment, 3) a representative meteor entry. Flow simulations for these problems have been performed using the LAURA non-equilibrium Navier-Stokes solver [29]. Next, LOSs along the forebody stagnation line and through the wake (starting from the backshell) are extracted. The non-equilibrium dynamics of the gaseous mixture are described using a two-temperature thermochemical model comprising of 11-species air (N, N^+, O, O^+, NO, NO^+, N_2, $N_2{}^+$, O_2, $O_2{}^+$, and e^-) and kinetic rates presented by Johnston and Panesi [30]. A quasi-steady solution (QSS) for the electronic states of atomic nitrogen is obtained prior to radiative transfer calculations, thereby accounting for non-Boltzmann effects on thermal radiation [31]. The freestream conditions for each of the three cases under study along with references detailing the computational setup, mesh configuration, and LOS properties are:

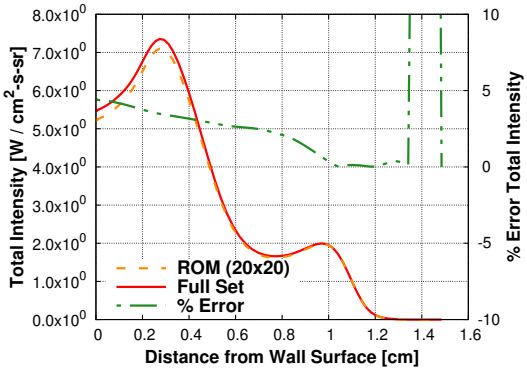

(a) Total intensity

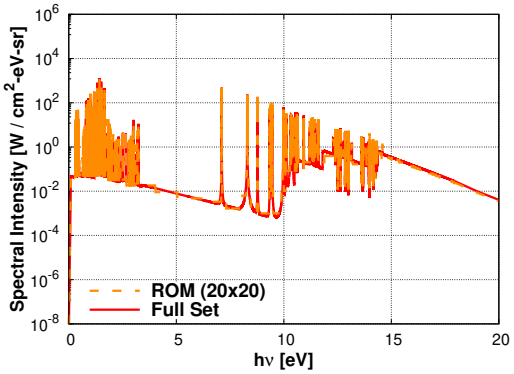

(b) Spectral intensity at the wall

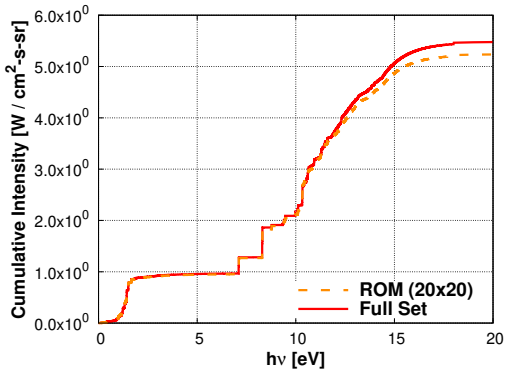

(c) Cumulative intensity at the wall

Fig. 1 Comparison of wall-directed intensities along the stagnation line during Stardust entry.

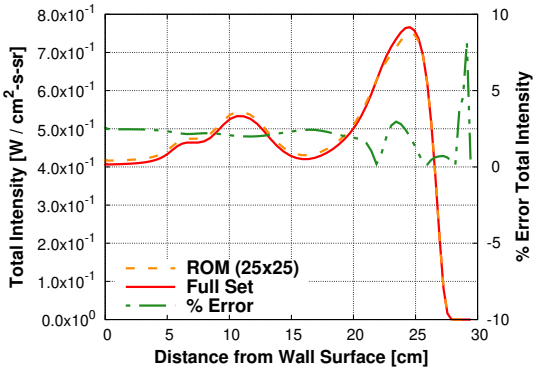

(a) Total intensity

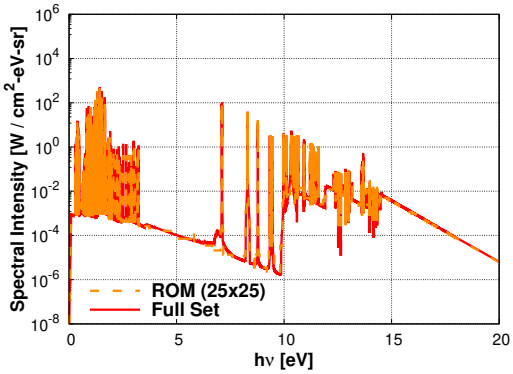

(b) Spectral intensity at the wall

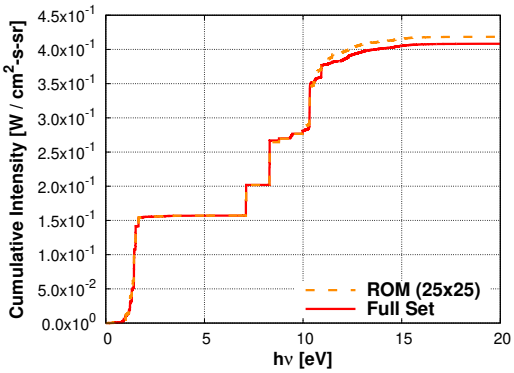

(c) Cumulative intensity at the wall

Fig. 2 Comparison of wall-directed intensities along a backshell LOS during Stardust entry.

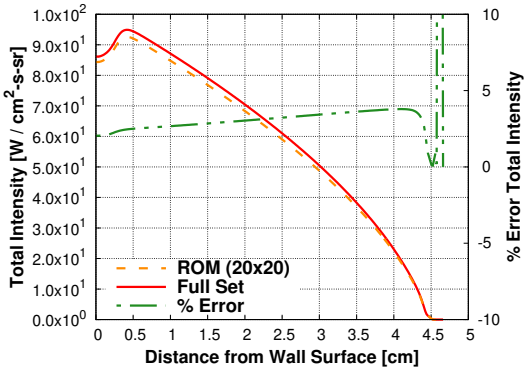

(a) Total intensity

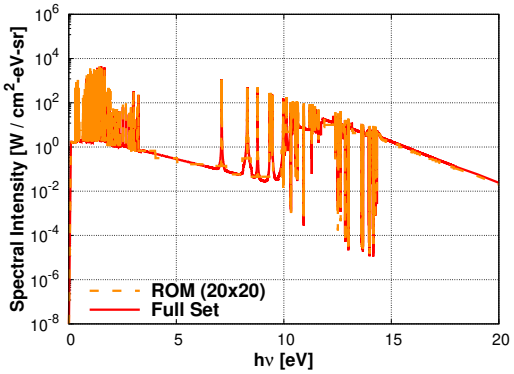

(b) Spectral intensity at the wall

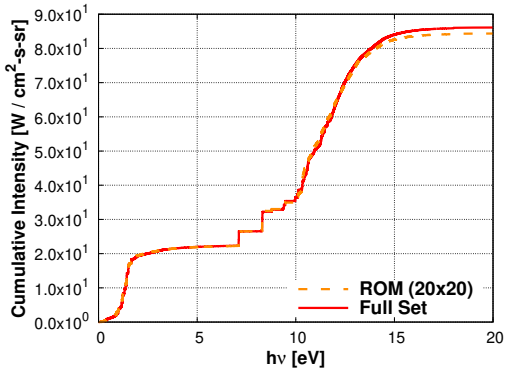

(c) Cumulative intensity at the wall

Fig. 3 Comparison of wall-directed intensities along the stagnation line during FIRE II entry.

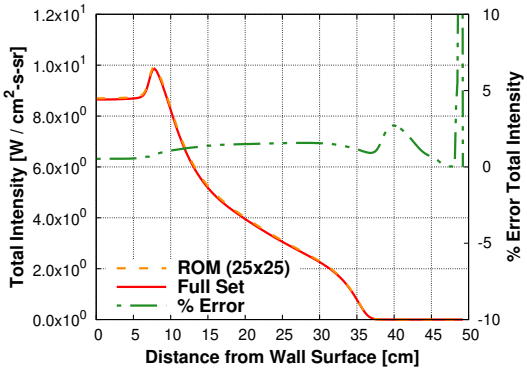

(a) Total intensity

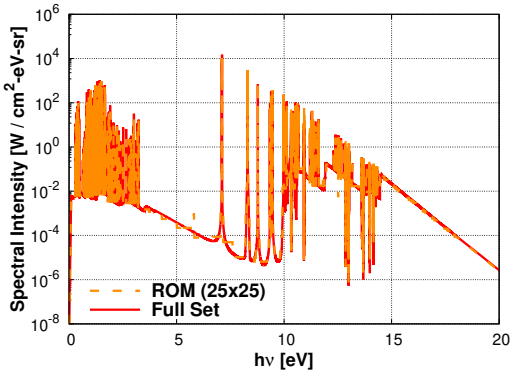

(b) Spectral intensity at the wall

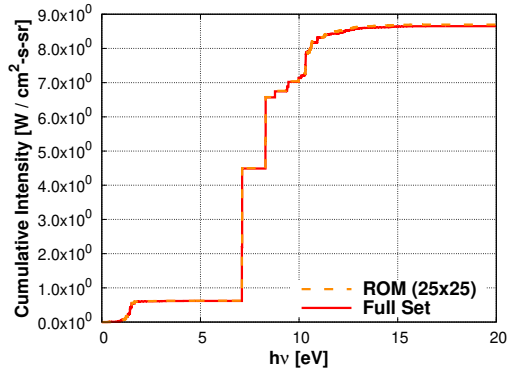

(c) Cumulative intensity at the wall

Fig. 4 Comparison of wall-directed intensities along a backshell LOS during FIRE II entry.

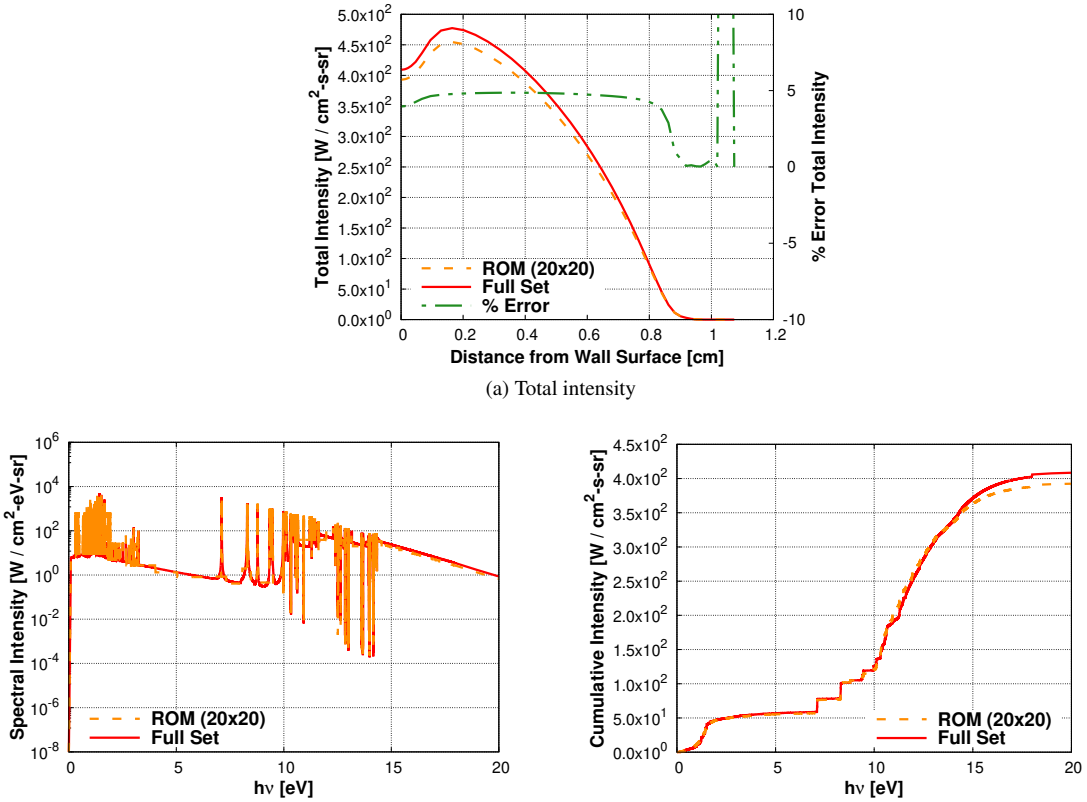

(a) Total intensity

(b) Spectral intensity at the wall

(c) Cumulative intensity at the wall

Fig. 5 Comparison of wall-directed intensities along the stagnation line during meteor entry.

1) Stardust entry has been analyzed at the 46 s trajectory point when freestream velocity $V_\infty = 11.69$ km/s and density $\rho_\infty = 1.05 \times 10^{-4}$ kg/m^3 [32].
2) FIRE II entry has been analyzed at the 1636 s trajectory point when freestream velocity $V_\infty = 11.31$ km/s and density $\rho_\infty = 8.57 \times 10^{-5}$ kg/m^3 [33].
3) Meteoroid radius of 1 m is assumed with atmospheric entry occurring at freestream velocity $V_\infty = 20$ km/s and an altitude of 50 km [34].

The frequency-integrated wall-directed radiative intensity along with spectral and cumulative intensities at the wall are compared for the reduced-order model and full set for the Stardust stagnation LOS in Fig. 1. It should be noted that the unpacking strategy discussed in [21, 22] is used to estimate frequency-wise intensity distributions from the reduced-order solutions. The reduced-order model for this LOS (also highlighted in Fig. 1) consists of $20 \times 20 = 400$ groups. Similar analysis for the Stardust wake, FIRE II stagnation and wake, and meteor stagnation LOSs are presented in figures 2-5. Radiative heating for such entry problems is shaped by a complex interplay of non-local and non-equilibrium effects. The total intensity is dominated by strong self-absorbing atomic lines and continuum emission. Radiation emanating from the shock layer (optically thickest for meteor entry) is absorbed in the boundary layer (larger for the wake LOSs). Furthermore, key atomic lines, such as the one located at 174 nm (7.1 eV), are strongly impacted by non-Boltzmann state populations. This is of particular import as large sections of the flowfield, through a combination of rapid expansion around the shoulder and proximity to the oblique shock, are in a state of strong thermochemical non-equilibrium.

The ROM database predicts radiative intensity with less than 5% error, indicative of the fundamental non-linear interactions being recreated correctly. This level of efficacy is maintained across the various entry cases and LOS locations, each with their distinct flow phenomenology and thermochemical characteristics, with no case-specific tuning. Another noteworthy outcome is the excellent agreement obtained for the frequency-wise intensity distribution with full set models. Prominent spectral features, especially the discrete peaks, are captured with a maximum of 25×25 evaluations (corresponding to the number of reduced-order groups) rather than the original $\tilde{1}00{,}000$ evaluations for the

full set. There is a slight mismatch in spectral intensity emanating from continuum processes in the [12, 15] eV region which needs to studied further. High-fidelity in the spectral space is imperative for delivering self-consistent coupled radiation models that can correctly model phenomena such photoionization and photodissociation. These processes can induce strong deviation from Boltzmann population distributions and noticeably alter radiative heat loads on vehicles.

B. 3D Orion Forebody

A 3D computational grid encompassing the forebody and extending just beyond the shoulder of the Orion spacecraft is utilized for the ensuing analysis. This volumetric domain is discretized using 10^6 hexahedral element. The freestream inflow is defined as $V_\infty = 10.5$ km/s, $\rho_\infty = 2.73 \times 10^{-4}$ kg/m^3, temperature $T_\infty = 244$ K, and angle of attack $\alpha_\infty = 18°$ which corresponds to peak heating lunar-return conditions [35]. A purely nitrogen-based gaseous mixture comprising of 5 species – N_2, N, N_2^+, N^+, and e^- – is assumed to speed-up simulations. Chemical kinetics rate and relaxation coefficients presented in [36] are utilized. Additionally, the walls of the spacecraft are assumed to be fully catalytic and in radiative equilibrium with an emissivity value of 0.85. Supersonic inflow or outflow are prescribed on the remaining boundary faces. The flow is considered to be laminar and no explicit turbulence modeling is incorporated in the results. A one-way coupling between the flow and radiation fields is considered; a steady-state flowfield solution is first obtained using US3D, followed by radiative transfer calculations using NERO.

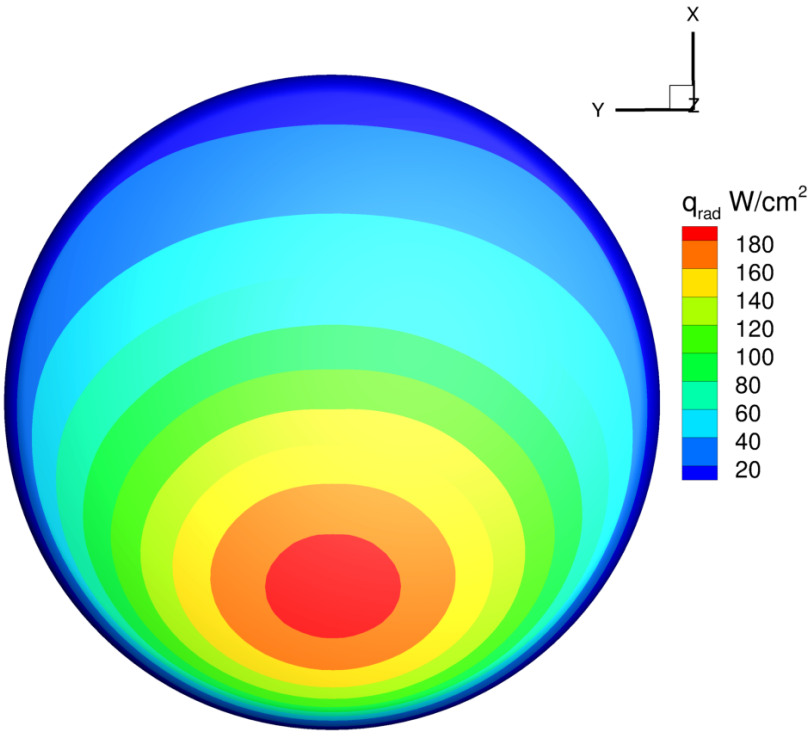

Fig. 6 Total 3D radiative heat flux on the Orion forebody surface computed using 625 reduced-order groups.

The total radiative heat flux due to atomic nitrogen received by the Orion forebody is presented in Fig. 6. Surface heating is maximum near the stagnation point and decreases away from it. Radiative transfer computations are based on a ROM database, same as the one for the previous LOS study, consisting of $25 \times 25 = 625$ reduced-order groups. A set of 86 of quadrature points is sufficient for converging angular integration. Both surface and volumetric radiative heating are resolved in approximately three minutes while running on 200 processors. On the other hand, legacy tools such as NEQAIR and HARA would require significantly more computational resources — ranging from roughly an hour for surface heat flux and tens of hours for volumetric heating – to tackle the same problem. Surface heating has also been calculated using HARA which relies on the LAURA CFD solver for the flow solution. Surface heating rates estimated by the NERO-US3D and HARA-LAURA frameworks are contrasted in Fig. 6. Good agreement is observed for the two sets of results with differences in incident heat flux not exceeding 7.5%, a value significantly lower than uncertainty bounds

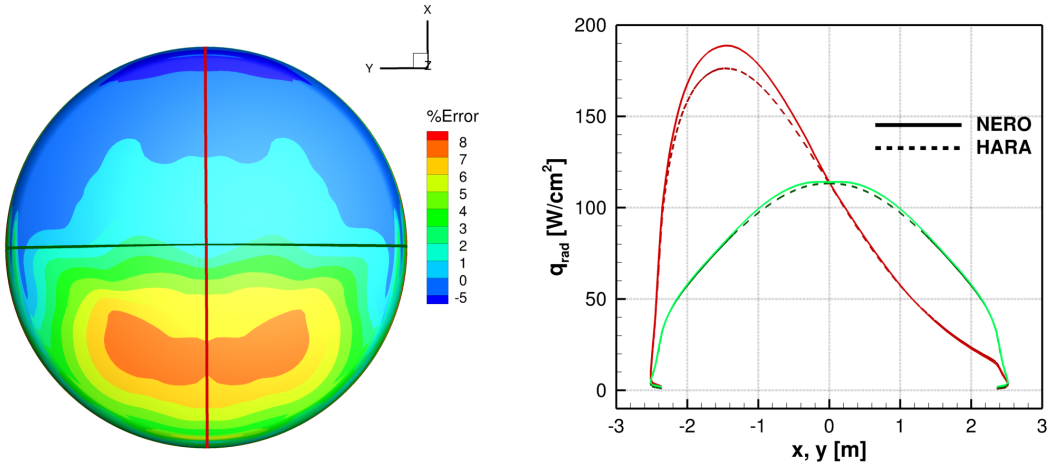

Fig. 7 Percentage difference in surface heating predicted using the NERO-US3D and HARA-LAURA frameworks (left). Heat flux values along the $x, y = 0$ edges are compared on the right.

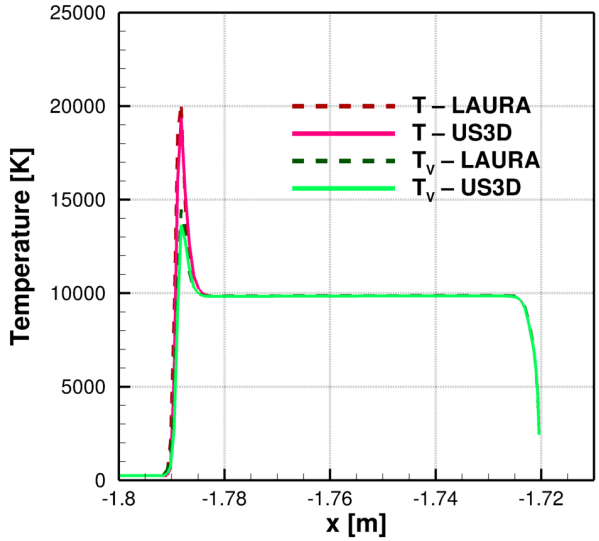

Fig. 8 Translational-rotational T and vibrational-electronic T_v temperatures along the stagnation line computed by the US3D and LAURA CFD solvers.

on concomitant modeling parameters. However, this still remains an incomplete examination of NERO's predictive capabilities vis-a-vis an extensively validated/verified legacy solver such as HARA. Notwithstanding the authors' best efforts to ensure congruity in terms of chemical kinetics, flowfield inputs, and computational setup, there are inherent dissimilarities between US3D and LAURA with regards to numerical schemes and treatment of boundary conditions and thermochemical effects. The same becomes evident in Fig. 8 which compares the translational-rotational T and vibrational-electronic T_v temperatures along the stagnation line. The maximum value of T_v in the shock layer differs by 6% between the two CFD solvers which further amplifies discrepancies in the resulting radiative fields. A stagnation LOS from the same flowfield when processed by both NERO and HARA returns virtually identical space variation in total intensity (percentage difference less than 1.5%) and spectral composition at the wall. The aforementioned analysis is performed on the stagnation line extracted from the US3D flowfield and is illustrated in Fig. 9. It adds further credence to the claim that despite the enormous advances in computational efficiency NERO retains the ability to reliably determine radiative characteristics with the same fidelity as legacy solvers.

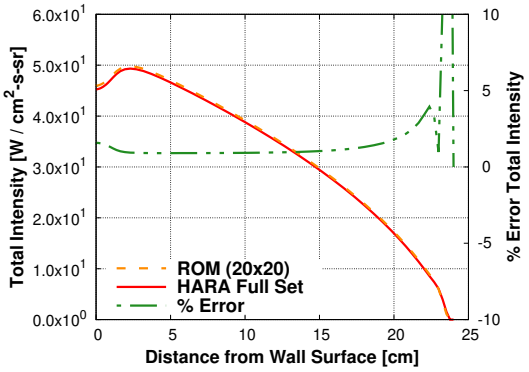

(a) Total intensity

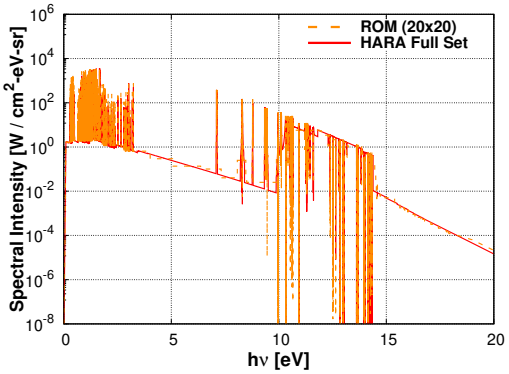

(b) Spectral intensity at the wall

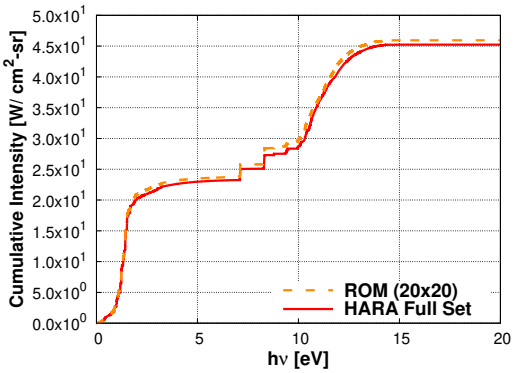

(c) Cumulative intensity at the wall

Fig. 9 Comparison of wall-directed intensities predicted using NERO and HARA radiation solvers along the stagnation line from the US3D flow solution.

IV. Conclusion

A new simulation framework has been developed for efficiently solving radiative heat transfer for complex non-equilibrium atmosphere entries. A key focus has been on ensuring computational efficiency and the ability to interface with unstructured, finite-volume CFD solvers. This has been done with the intent of making high-fidelity aerothermal analysis with strong flow-radiation coupling readily available during mission design and trade studies. The system of RTEs corresponding to a given direction is first discretized through standard finite volume simplifications. Surface fluxes are computed using first-order unwinding which ensures positivity and boundedness. The resulting sparse system of linear equations is subjected to mesh reordering, thereby allowing intensity at cell-centers to be updated using an inexpensive explicit closed-form expression. The approximation of angular integration over the complete solid angle is based on the discrete ordinate method and Lebedev-type quadrature rules. The multi band-bin reduced-order method is employed which involves combining individual frequencies (from detailed radiation databases) into larger groups. The absorptivity of reduced-order group is obtained using the Planck-averaging maximum entropy closure. Furthermore, a new methodology has been evolved which allows the model-reduction process to be completed *a priori* to actual simulations and requires no flowfield information as input.

The new model-reduction approach has been applied to the atomic nitrogen radiative system, resulting in a ROM database with three orders-of-magnitude fewer spectral points and a 95% reduction in memory requirements. The accuracy of the reduced-order system has been benchmarked first on different LOSs from Stardust, FIRE II, and meteory entry flow solutions. This is followed by calculation of 3D radiative heat flux on the Orion forebody and a comparison with predictions from the HARA-LAURA framework. Both total radiative heat flux and detailed spectral features are consistently recovered with less than 5% difference with respect to full set/HARA predictions. The performance gains from the new framework pave the way for rigorous characterization of vehicular heating while accounting for complex features such as antennas, recesses, and seals, which would directly translate into aggressive, focused design

margins. Furthermore, the modular structure established for NERO ensures that it can work in tandem with other unstructured mesh-based tools – material response codes [37], particle solvers for dust-laden flows [38], and optimization frameworks [39] – in a multi-physics hypersonic software suite. A key objective that needs to be pursued next is the generation of similar ROM databases for radiative systems such as atomic oxygen, CN-Red, and CN-Violet that are relevant to upcoming NASA missions. Another aspect that requires rumination (and possible modifications to the spectral model-reduction procedure) is concurrently dealing with multiple radiative systems that overlap in the frequency domain.

Acknowledgments

This work has been supported by the Entry Systems Modeling project under the NASA Game Changing Development program. Additionally, support for Amal Sahai was provided under NASA contract NNA15BB15C to AMA, Inc.

References

[1] Dillman, R. A., and Corliss, J. M., "Overview of the Mars sample return Earth entry vehicle," *6th International Planetary Probe Workshop*, 2008.

[2] Brandis, A. M., Saunders, D. A., Allen, G. A., Stern, E. C., Wright, M. J., Mahzari, M., Johnston, C. O., Hill, J. P., Adams, D. S., and Lorenz, R. D., "Aerothermodynamics for Dragonfly's Titan Entry," *15th International Planetary Probe Workshop*, 2018.

[3] Yoon, S., Gnoffo, P. A., White, J., and Thomas, J., "Computational challenges in hypersonic flow simulations," *39th AIAA Thermophysics Conference*, Vol. AIAA Paper 2007-4265, 2007.

[4] Brandis, A. M., Saunders, D. A., Johnston, C. O., Cruden, B. A., and White, T. R., "Radiative heating on the after-body of Martian entry vehicles," *Journal of Thermophysics and Heat Transfer*, Vol. 34, No. 1, 2020, pp. 66–77.

[5] Brandis, A. M., and Cruden, B. A., "NEQAIRv14.0 Release Notes: Nonequilibrium and Equilibrium Radiative Transport Spectra Program," Technical Report, NASA Ames Research Center, 2014.

[6] Johnston, C. O., Hollis, B. R., and Sutton, K., "Spectrum modeling for air shock-layer radiation at lunar-return conditions," *Journal of Spacecraft and Rockets*, Vol. 45, No. 5, 2008, pp. 865–878.

[7] Mazaheri, A., Johnston, C. O., and Sefidbakht, S., "Three-Dimensional Radiation Ray-Tracing for Shock-Layer Radiative Heating Simulations," *Journal of Spacecraft and Rockets*, Vol. 50, No. 3, 2013, pp. 485–493.

[8] Lamet, J.-M., Babou, Y., Riviere, P., Perrin, M.-Y., and Soufiani, A., "Radiative transfer in gases under thermal and chemical nonequilibrium conditions: Application to Earth atmospheric re-entry," *Journal of Quantitative Spectroscopy and Radiative Transfer*, Vol. 109, No. 2, 2008, pp. 235–244.

[9] Brewster, M. Q., *Thermal radiative transfer and properties*, John Wiley & Sons, 1992.

[10] Candler, G. V., Johnson, H. B., Nompelis, I., Gidzak, V. M., Subbareddy, P. K., and Barnhardt, M., "Development of the US3D code for advanced compressible and reacting flow simulations," Vol. AIAA Paper 2015-1893, 2015.

[11] Modest, M. F., *Radiative heat transfer*, Academic Press, 2013.

[12] Coelho, P. J., "A comparison of spatial discretization schemes for differential solution methods of the radiative transfer equation," *Journal of Quantitative Spectroscopy and Radiative Transfer*, Vol. 109, No. 2, 2008, pp. 189–200.

[13] Lebedev, V. I., "Quadratures on a sphere," *USSR Computational Mathematics and Mathematical Physics*, Vol. 16, No. 2, 1976, pp. 10–24.

[14] Miranda, F. C., di Mare, F., Sadiki, A., and Janicka, J., "Performance analysis of different solvers for computing the radiative transfer equation in complex geometries using finite volume method and block structured grids," *Computational Thermal Sciences: An International Journal*, Vol. 9, No. 3, 2017.

[15] Asllanaj, F., Contassot-Vivier, S., Liemert, A., and Kienle, A., "Simulation of light propagation in biological tissue using a modified finite volume method applied to three-dimensional radiative transport equation," *European Conference on Biomedical Optics*, 2015.

[16] Moens, N., Sundqvist, J., El Mellah, I., Poniatowski, L., Teunissen, J., and Keppens, R., "Radiation-hydrodynamics with MPI-AMRVAC-Flux-limited diffusion," *Astronomy & Astrophysics*, Vol. 657, 2022, p. A81.

[17] Wray, A., "Improved Finite-Volume Method for Radiative Hydrodynamics," *7th International Conference on Computational Fluid Dynamics*, 2012.

[18] Sahai, A., Lopez, B., Johnston, C. O., and Panesi, M., "Flow-radiation coupling in CO_2 hypersonic wakes using reduced-order non-Boltzmann models," *Physical Review Fluids*, Vol. 4, No. 9, 2019, p. 093401.

[19] Sahai, A., "Reduced-order modeling of non-Boltzmann thermochemistry and radiation for hypersonic flows," Phd Thesis, University of Illinois at Urbana-Champaign, 2019.

[20] Joseph, D., El Hafi, M., Fournier, R., and Cuenot, B., "Comparison of three spatial differencing schemes in discrete ordinates method using three-dimensional unstructured meshes," *International Journal of Thermal Sciences*, Vol. 44, No. 9, 2005, pp. 851–864.

[21] Johnston, C. O., Sahai, A., and Panesi, M., "Extension of Multiband Opacity-Binning to Molecular, Non-Boltzmann Shock Layer Radiation," *Journal of Thermophysics and Heat Transfer*, 2017, pp. 1–6.

[22] Sahai, A., Johnston, C. O., Lopez, B., and Panesi, M., "Comparative analysis of reduced-order spectral models and grouping strategies for non-equilibrium radiation," *Journal of Quantitative Spectroscopy and Radiative Transfer*, Vol. 242, 2020, p. 106752.

[23] Karl, S., Potter, D., Lambert, M., and Hannemann, K., "Computational Analysis of Radiative Heat Loading on Hypervelocity Reentry Vehicles," *Journal of Spacecraft and Rockets*, Vol. 52, No. 1, 2014, pp. 63–75.

[24] Sahai, A., Lopez, B., Johnston, C. O., and Panesi, M., "Adaptive coarse graining method for energy transfer and dissociation kinetics of polyatomic species," *The Journal of Chemical Physics*, Vol. 147, No. 5, 2017, p. 054107.

[25] Turpault, R., "A consistent multigroup model for radiative transfer and its underlying mean opacities," *Journal of Quantitative Spectroscopy and Radiative Transfer*, Vol. 94, No. 3-4, 2005, pp. 357–371.

[26] Haut, T. S., Ahrens, C. D., Jonko, A., Till, A. T., and Lowrie, R. B., "Resolving Rapid Variation in Energy for Particle Transport," Technical Report, Los Alamos National Laboratory, 2016.

[27] Scoggins, J. B., Magin, T., Wray, A. A., and Mansour, N., "Multi-group reductions of LTE air plasma radiative transfer in cylindrical geometries," *AIAA Paper*, 2013, p. 3142.

[28] Johnston, C. O., "Nonequilibrium shock-layer radiative heating for Earth and Titan entry," Phd Thesis, Virginia Polytechnic Institute and State University, 2006.

[29] Mazaheri, A., Gnoffo, P. A., Johnston, C. O., and Kleb, B., "LAURA Users Manual: 5.5-65135," *NASA TM 2013-217800*, 2013.

[30] Johnston, C., and Panesi, M., "Advancements in afterbody radiative heating simulations for Earth entry," *46th AIAA Thermophysics Conference*, Vol. AIAA Paper 2016-3693, 2016.

[31] Johnston, C. O., Hollis, B. R., and Sutton, K., "Non-Boltzmann modeling for air shock-layer radiation at lunar-return conditions," *Journal of Spacecraft and Rockets*, Vol. 45, No. 5, 2008, pp. 879–890.

[32] Johnston, C. O., and Panesi, M., "Impact of state-specific flowfield modeling on atomic nitrogen radiation," *Physical Review Fluids*, Vol. 3, No. 1, 2018, p. 013402.

[33] Johnston, C. O., and Brandis, A. M., "Features of afterbody radiative heating for Earth entry," *Journal of Spacecraft and Rockets*, Vol. 52, No. 1, 2015, pp. 105–119.

[34] Johnston, C. O., Stern, E. C., and Wheeler, L. F., "Radiative heating of large meteoroids during atmospheric entry," *Icarus*, Vol. 309, 2018, pp. 25–44.

[35] Kleb, B., and Johnston, C. O., "Uncertainty analysis of air radiation for Lunar return shock layers," *AIAA Atmospheric Flight Mechanics Conference and Exhibit*, Vol. AIAA Paper 2008-6388, 2008.

[36] Park, C., "Review of chemical-kinetic problems of future NASA missions. I-Earth entries," *Journal of Thermophysics and Heat transfer*, Vol. 7, No. 3, 1993, pp. 385–398.

[37] Schulz, J. C., Stern, E., Muppidi, S., Palmer, G., Schroeder, O., and Martin, A., "Development of a three-dimensional, unstructured material response design tool," *55th AIAA Aerospace Sciences Meeting*, Vol. AIAA Paper 2017-0667, 2017.

[38] Sahai, A., and Palmer, G. E., "Variable-fidelity Euler–Lagrange framework for simulating particle-laden high-speed flows," *AIAA Journal*, Vol. 60, No. 5, 2022, pp. 3001–3019.

[39] Sahai, A., John, B., and Natarajan, G., "Effect of fineness ratio on minimum-drag shapes in hypersonic flows," *Journal of Spacecraft and Rockets*, Vol. 51, No. 3, 2014, pp. 900–907.